Proceedings of the ASME 2013 International Mechanical Engineering Congress and Exposition
IMECE2013
November 15-21, 2013, San Diego, California, USA

IMECE2013-63801

STRATIFICATION IN ISOTHERMAL ICE-SLURRY PIPE FLOW

Charles Landa Onokoko
Génie mécanique, Université de Sherbrooke
Sherbrooke, Qc, Canada J1K2R1

Nicolas Galanis
Génie mécanique, Université de Sherbrooke
Sherbrooke, Qc, Canada J1K2R1

ABSTRACT

A single-phase 3D model for isothermal laminar and turbulent flow of an ice slurry in a horizontal pipe is used to investigate the effects of the uniform inlet velocity and ice concentration on their axial evolution. The slurry is modeled as a Newtonian fluid with effective local properties depending on the local ice concentration. Despite the relative simplicity of this model (compared to the two-phase models used elsewhere) its numerical solution gives results which correctly reflect experimental observations. Specifically, these results show that as the fluid moves downstream the ice concentration increases in the upper part of the pipe and it decreases in the lower part. The velocity profile is principally influenced by the boundary layer growth close to the inlet but further downstream it becomes asymmetrical with respect to the horizontal symmetry plane with higher velocities in the lower part of the pipe. The differences between the values in the upper and lower parts of the pipe are much more important in the case of laminar flow. The results are analyzed by considering the phenomena influencing the ice particle movement (buoyancy and diffusion) and the relation between ice concentration and the thermophysical properties of the slurry.

INTRODUCTION

Ice slurries are mixtures of small ice particles (typically 0.1 to 1 mm of diameter) and a carrier liquid (a mixture of water and an additive such as glycol, sodium chloride or calcium carbonate which lowers the freezing temperature). They offer the possibility of enhanced energy transport density and energy storage due to the combined effects of sensible and latent heat. Applications include comfort cooling of buildings, food processing and the replacement of secondary refrigerants in ice rinks or supermarkets. Their thermophysical properties can be derived from linear weighing of the corresponding properties of the ice (which are essentially determined by the temperature) and the carrier liquid (which vary with the temperature and the concentration of the additive) [1].

The behavior of ice slurries in heat transfer installations is complex. Thus, in horizontal pipes separation of the solid ice particles and carrier liquid occurs with any particle size at very low velocities and with large particles at high velocities. Various flow patterns can be encountered in ice slurry pipelines that affect the hydrodynamics of the flow and the mechanism of heat transfer. The different experimentally observed flow patterns are classified as homogeneous, heterogeneous, sliding bed and stationary bed [1]. Kitanovski & Poredos [2] calculated the concentration distribution of ice in horizontal pipe flow by integrating the one-dimensional diffusion equation with constant values of the diffusion coefficient and the hindered settling velocity of the ice particles. They then calculated the average ice slurry viscosity by integrating the well-known Thomas equation applied locally with the calculated concentration profile. They concluded that for high average velocities and very low ice concentrations “the ice slurry viscosity is almost independent of velocity as for Newtonian fluids”. On the other hand, ice slurries exhibit a non-Newtonian behavior for ice concentrations exceeding approximately 20 % but this threshold value is also influenced by parameters such as the size of the ice particles and the nature of the additive. Several experimental studies have determined values of the effective viscosity of ice slurries and compared them with different rheological models [3].

Several CFD analyses of slurry flow with or without heat transfer have been published in recent years. Thus, Jihong Wang et al [4] applied an Euler-Euler model and calculated profiles of velocity and ice particle concentration as well as pressure drop for turbulent isothermal flow in horizontal, vertical and 90º elbow pipes. Their numerical predictions are within 20% of corresponding measured values. Niezgoda-Zelasko & Zalewski [5] obtained numerical results using a single-phase model with a Bingham fluid and multiphase models (mixture and Eulerian models). They found that for laminar flows both the Bingham and mixture models gave a correct description of the flow field. For low Reynolds number

turbulent flows they found that the best agreement between numerical and experimental results (for the single-phase and the multiphase Eulerian models) was obtained by using the RNG k-ε turbulence model with the enhanced wall treatment.

In the present study we consider the isothermal, steady, laminar and turbulent flows of ice slurry in the entrance region of a horizontal pipe. The ice slurry is treated as a single phase Newtonian fluid with effective properties. A model consisting of the three-dimensional differential equations of motion for the slurry, the realizable k-ε turbulence model as well as the conservation equation for the ice particles is proposed and solved numerically. These equations are coupled since the viscosity and density of the slurry depends on the ice concentration which changes from the assumed uniform distribution at the inlet due to the opposing effects of buoyancy and diffusion. The results illustrate the axial evolution of the ice concentration and the velocity profiles which depend on the flow regime (laminar or turbulent) and are in good qualitative agreement with experimental observations.

DESCRIPTION AND MODELING OF THE PROBLEM

The ice slurry under consideration is an aqueous solution of ethylene glycol and ice particles of mean diameter d. It is flowing in a horizontal adiabatic pipe of diameter D and length $L = 300\ D$. At the pipe inlet the velocity V_0, the temperature T_0 and the volumetric concentration $\emptyset_0$ of the ice particles are uniform. The outflow condition is applied at the pipe outlet. The no-slip and no-ice particle-flux are applied at the pipe wall. The origin of the coordinates system is at the pipe inlet. The z axis coincides with the pipe axis while the x and y axes are horizontal and vertical respectively.

Laminar flow

The governing equations are based on the continuum approach. The ice particles migration that includes several mechanisms (Brownian motion, particle settling, shear-induced, and viscosity gradients migration) is described by an additional transport equation.

The steady state continuity and momentum conservation equations are given respectively by:

$$\boldsymbol{\nabla} \cdot (\rho_{is} \boldsymbol{u}) = 0 \tag{1}$$

$$\boldsymbol{\nabla} \cdot (\rho_{is} \boldsymbol{u}\boldsymbol{u}) = -\boldsymbol{\nabla} p + \boldsymbol{\nabla} \cdot \boldsymbol{\tau} \tag{2}$$

The steady state species conservation equation, based on the particle diffusive model proposed by Phillips et al. [6], is

$$\boldsymbol{\nabla} \cdot (\ \rho_{is} \boldsymbol{u} \emptyset) = -\boldsymbol{\nabla} \cdot \boldsymbol{N_t} \tag{3}$$

This equation represents a balance between the convective and diffusive particle flux. Neglecting Brownian motion, we model the diffusive particle flux as:

$$\boldsymbol{N_t} = \boldsymbol{N_c} + \boldsymbol{N_\mu} + \boldsymbol{N_s} \tag{4}$$

Where $\boldsymbol{N_c}$ is the flux induced by the gradients of shear rate, $\boldsymbol{N_\mu}$ is the flux due to spatial variation in viscosity, and $\boldsymbol{N_s}$ is the flux due to particle settling. Based on the scaling arguments of Leighton & Acrivos [7], Phillips et al. [6] proposed the following expressions:

$$\boldsymbol{N_c} = -\rho_{is} K_c a^2 (\emptyset^2 \boldsymbol{\nabla}\dot{\gamma} + \dot{\gamma}\emptyset \boldsymbol{\nabla}\emptyset) \tag{5a}$$

$$\boldsymbol{N_\mu} = -\rho_{is} K_\mu a^2 \dot{\gamma} \emptyset^2 \frac{1}{\mu_{is}} \frac{d\mu_{is}}{d\emptyset} \boldsymbol{\nabla}\emptyset \tag{5b}$$

The values of the coefficients are $K_c = 0.41$ and $K_\mu = 0.62$.
For the settling particle flux we adopt the following form proposed by Richardson & Zaki [8]:

$$\boldsymbol{N_s} = \rho_{is} \omega_0 f(\emptyset) \emptyset \boldsymbol{Q} \tag{5c}$$

Where ω_0 is the terminal settling velocity of a single particle in the aqueous solution and $f(\emptyset)$ is the hindrance function. For the latter we adopt the form suggested by Revay & Higdon [9]:

$$f(\emptyset) = (1 - \emptyset)^{6.55}(1 + 3.458\emptyset^2 + 8.990\emptyset^3) \tag{5d}$$

With these relations the species conservation equation becomes

$$\boldsymbol{\nabla} \cdot \{\rho_{is}[\boldsymbol{u} + \omega_0 f(\emptyset)\boldsymbol{Q}]\emptyset\} = \boldsymbol{\nabla} \cdot (\Gamma \boldsymbol{\nabla}\emptyset) + \boldsymbol{S} \tag{6a}$$

The diffusive coefficient Γ and the source term $\boldsymbol{S}$ are:

$$\Gamma = \rho_{is} a^2 \emptyset \dot{\gamma} \left(K_c + K_\mu \emptyset \frac{\partial \mu_{is}}{\mu_{is} \partial \emptyset}\right) \tag{6b}$$

$$\boldsymbol{S} = \boldsymbol{\nabla} \cdot (\rho_{is} \mathrm{K_c a^2} \emptyset^2 \boldsymbol{\nabla}\dot{\gamma}) \tag{6c}$$

Turbulent flow

For steady state conditions the averaged equations of mass conservation and momentum are:

$$\frac{\partial}{\partial x_i}(\rho_{is} \bar{u}_i) = 0 \tag{7}$$

$$\frac{\partial}{\partial x_j}(\rho_{is} \bar{u}_i \bar{u}_j) = -\frac{\partial \bar{P}}{\partial x_i} + \frac{\partial}{\partial x_j}\left[\mu_{is}\left(\frac{\partial \bar{u}_i}{\partial x_j} + \frac{\partial \bar{u}_i}{\partial x_i} - \frac{2}{3}\delta_{ij}\frac{\partial \bar{u}_i}{\partial x_i}\right)\right] + \frac{\partial}{\partial x_j}\left(-\rho_{is}\overline{u_i' u_j'}\right) \tag{8}$$

The turbulence model adopted in the present study is the realizable k-ε model. It was preferred to the standard k-ε model because it includes an improved equation for ε and uses a variable coefficient in the expression of the turbulent viscosity. It is appropriate for boundary layers with strong adverse pressure gradients such as those encountered near the inlet in the problem under consideration. The corresponding equations are:

$$\frac{\partial}{\partial x_i}(\rho_{is} k \bar{u}_i) = \frac{\partial}{\partial x_i}\left[\left(\mu_{is} + \frac{\mu_t}{\rho_k}\right)\frac{\partial k}{\partial x_i}\right] + G_k + G_b - \rho_{is}\varepsilon - Y_m + S_k \tag{9a}$$

$$\frac{\partial}{\partial x_i}(\rho_{is} \varepsilon \bar{u}_i) = \frac{\partial}{\partial x_i}\left[\left(\mu_{is} + \frac{\mu_t}{\rho_\varepsilon}\right)\frac{\partial \varepsilon}{\partial x_i}\right] + \rho_{is} G_1 S_\varepsilon - \rho_{is} C_2 \frac{\varepsilon^2}{k + \sqrt{\nu\varepsilon}} + C_{1\varepsilon}\frac{\varepsilon}{k} C_{3\varepsilon}\ G_b + S_\varepsilon \tag{9b}$$

The particle diffusive model proposed by Phillips et al. [6] is also valid for turbulent conditions according to Bui et al [10]. When associated with the motion created by the density difference between the liquid and solid phases it results in the following expression for the species conservation equation:

$$\frac{\partial}{\partial x_i}\left[\rho_{is}\left(\bar{u}_i + \delta_{i3}\omega_0 f(\emptyset)\right)\emptyset\right] = \frac{\partial}{\partial x_i}\left[\Gamma_\emptyset \left(\frac{\partial \emptyset}{\partial x_i}\right)\right] + S_\emptyset \quad (10)$$

The diffusive coefficient Γ, the source term S, the hindrance function $f(\emptyset)$ and the values of the coefficients K_c and K_μ are identical to those for laminar flow.

Ice slurry properties

The fusion temperature of aqueous solutions of additives such as ethylene glycol decreases as the concentration of the additive (X_0 in kg of additive per kg of mixture or $\emptyset_0$ in m^3 of additive per m^3 of mixture) increases. For temperatures above this fusion temperature the mixture does not contain any ice particles. For temperatures below this fusion temperature the mixture contains solid particles which are considered to be pure water; as a result, for such temperatures, the concentration of additive in the liquid mixture is higher than X_0 (and $\emptyset_0$).

According to the Handbook on Ice Slurries [1] the density of the ice (subscript i) can be calculated from the expression:

$$\rho_i = 917 - 0.13T \quad (11)$$

The density and the viscosity of the liquid mixture of water and additive (subscript l) depend on the temperature and on the volumetric concentration of the additive (subscript a). They can be calculated from the following formulas:

$$\rho_l(\emptyset_a, T) = \sum_{i=0}^{M} T^i \sum_{j=0}^{N} b_{i,j}\emptyset_a^j$$

$$\mu_l(\emptyset_a, T) = \sum_{i=0}^{M} T^i \sum_{j=0}^{N} b_{i,j}\emptyset_a^j$$

The coefficients $b_{i,j}$ were calculated [11] by polynomial curve-fitting of tabulated data [12].

Finally, the density and viscosity of the ice slurry (subscript is) can be calculated from the following equations:

$$\rho_{is} = \emptyset\rho_i + (1-\emptyset)\rho_l \quad (13a)$$

$$\mu_{is} = \mu_l\left(1 + 2.5\emptyset + 10.05\emptyset^2 + 0.00273e^{16.6\emptyset}\right) \quad (13b)$$

In all the above expressions the density is in kg/m^3, the viscosity is in mPa s while T is the temperature in ºC.

SOLUTION AND VALIDATION

The coupled differential equations of the model were solved using the software Ansys-Fluent which is based on the finite volume technique. The ice particle conservation equation was introduced using the user-defined scalar functionality. The SIMPLE algorithm was employed to resolve the pressure-velocity coupling in the momentum equation. The QUICK scheme was used to approximate the convection term. The validation of the model was obtained by first simulating the steady laminar forced convection of water in a horizontal tube. Mesh independence was established by refining a coarser size until results were unchanged. Table 1 shows the calculated values of the non-dimensional velocity (V/V_0) at different axial positions (z*=(z/D)/Re) for three meshes and compares them with those obtained by Nascimento et al. [13] and Liu [14]. The fine mesh with approximately 7.1 10^6 cells which gives results in excellent agreement with the literature has been used to obtain all the results presented in the subsequent sections.

	z* = 0.0002116	z* = 0.005288	z* = 0.06281	z* = 0.08993
Coarse mesh (2169000 cells)	1.0359	1.4150	1.9777	1.9872
Medium Mesh (3481885 cells)	1.0108	1.3924	1.9791	1.9987
Fine Mesh (7117986 cells)	1.0094	1.4119	1.9802	1.9998
Liu [14]	1.100	1.439	1.989	1.999
Nascimento et al [13]	1.113	1.427	1.961	1.972

Table 1: Mesh independence tests and validation (Re=500, Water Flow)

For further validation the predicted velocity for a slurry with solid polypropylene spheres is compared in Fig. 1 with experimental results by Stutz et al [15]. The agreement is good. The differences are due to the fact that simulations were carried out by assuming that the carrying fluid is a mixture (water and 10% ethanol) while in the experiments it was pure water.

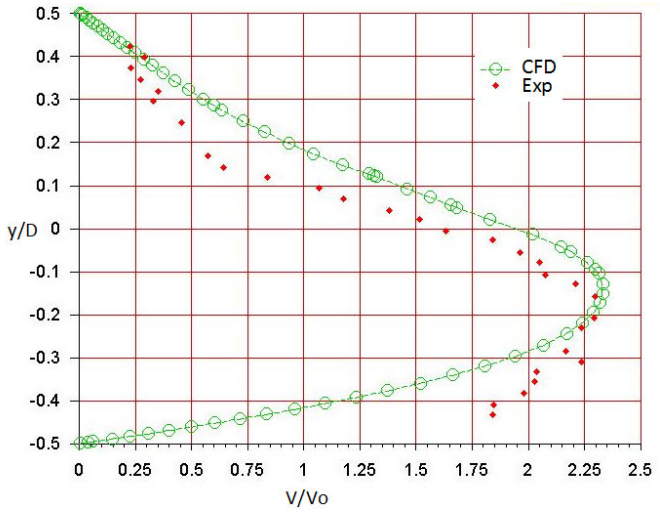

Fig. 1: Experimental and numerical velocity profiles

RESULTS AND DISCUSSION

Two series of simulations were carried out with different combinations of the inlet velocity and the inlet ice concentration. In all cases the additive is ethylene glycol with a mass concentration in the absence of ice equal to 14% (the corresponding fusion temperature is 268.24 K). The average diameter of the ice particles is d = 0.4 mm and the length of the pipe is L = 3 m for all simulations. The combinations of inlet velocity and inlet ice concentration are chosen so that the corresponding Reynolds number Re_0 is clearly in the laminar or turbulent regime. Specifically Re_0 is always less than 1000 for the first series and always more than 3000 for the second one.

Results for laminar flow

Figure 2 shows the axial evolution of the ice particles concentration distribution along the vertical diameter of the pipe for V_0 = 0.2 m/s and $\varnothing_0$ = 0.1 (which corresponds to a temperature of 267.56 K, i.e. slightly lower than the fusion temperature). Under the effect of buoyancy the ice particles whose density is smaller than that of the liquid mixture rise towards the top of the pipe. As a result of this phenomenon the ice particle concentration increases in the upper part of the pipe and it decreases in its lower part. The ensuing concentration gradient creates a downwards flux of ice particles which eventually becomes equal to the upward one sustained by buoyancy. Therefore the concentration profile eventually reaches a form which is independent of the axial position as illustrated by the fact that the profile at z = 1.50 m is identical to the one at z = 2.95 m.

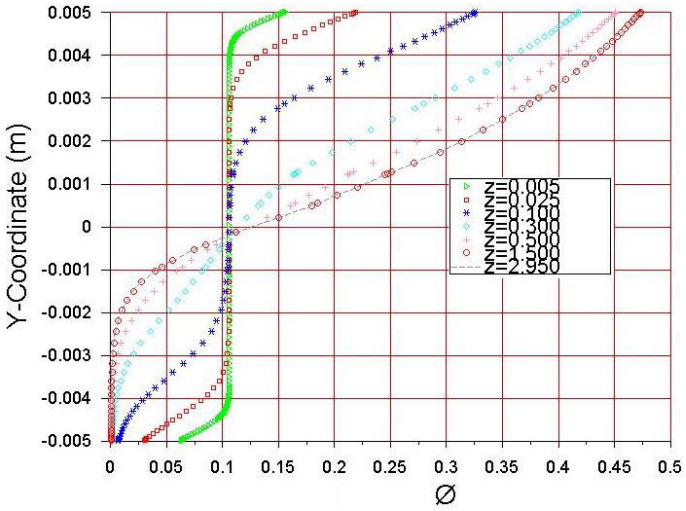

Fig. 2: Axial evolution of the concentration profile for V_0 = 0.2 m/s and $\varnothing_0$ = 0.1

Figure 3 shows the corresponding profiles of the axial velocity which also evolve with the distance from the inlet. Near the inlet (z = 0.005 m) we observe the well-known overshoot phenomenon caused by the rapid development of the boundary layer. Further downstream the velocity profile is not symmetrical with respect to the pipe axis. This is due to the influence of the ice particle concentration on the viscosity of the slurry. Thus, in the lower part of the pipe where the ice concentration is low the viscosity decreases and the velocity increases. On the other hand, in the higher part of the pipe where the ice concentration is high the viscosity increases and the velocity decreases. Eventually the velocity profile reaches a form which is independent of the axial position as illustrated by the fact that the profile at z = 1.50 m is identical to the one at z = 2.95 m.

It is therefore evident that for the conditions under consideration the flow field is fully developed beyond z=1.5 m.

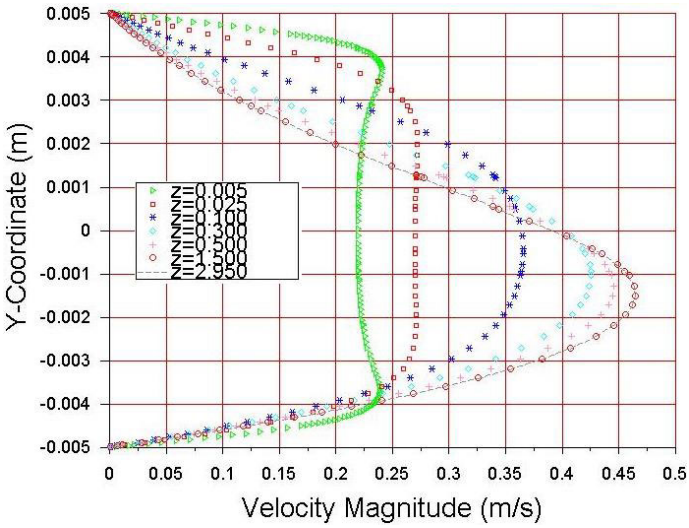

Fig. 3: Axial evolution of the velocity profile for V_0 = 0.2 m/s and $\varnothing_0$ = 0.1

In order to test the validity and precision of these results we calculated the average concentration of the ice particles for different cross sections normal to the pipe axis. This quantity was obtained by first integrating the product of the local ice concentration (function of x and y) and the local mass flowrate (also a function of x and y) over the circular cross section; this product was then divided by the mass flowrate of the ice slurry which is of course independent of the axial position. The comparison of the calculated values of the average concentration shows that this quantity is essentially independent of the axial position (see Table 2). This result was of course anticipated since the flow under consideration takes place without heat transfer and therefore the quantity of ice transported downstream should not change. The fact that the numerical results satisfy this condition is therefore an indication that the model and its numerical solution are reliable.

Axial position z (m)	0.05	0.5	1.0	2.0	2.95
Average ice concentration (%)	10.00	9.99	10.00	10.03	10.05

Table 2: Validation of the constancy of the average ice concentration for laminar flow

Figure 4 illustrates the effect of the inlet ice concentration on the fully developed concentration profile for V_0 = 0.35 m/s. We note that the lower part of the pipe does not contain any ice and that the vertical dimension of this ice-free region decreases as $\emptyset_0$ increases. Furthermore as $\emptyset_0$ increases the maximum concentration, which occurs at the top of the pipe, increases as well. These tendencies are consistent with experimental observations [1].

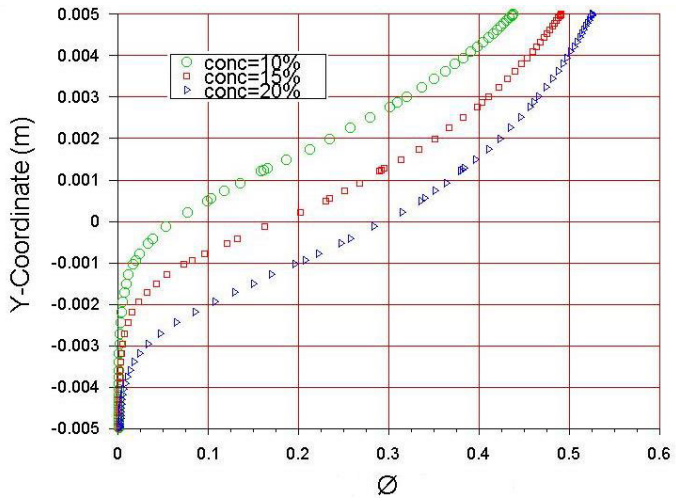

Fig. 4: Effect of $\emptyset_0$ on the fully developed concentration profile for V_0 = 0.35 m/s.

Figure 5 illustrates the effect of the inlet ice concentration on the fully developed velocity profile for V_0 = 0.35 m/s. We note that the increase of $\emptyset_0$ causes the increase of the maximum axial velocity and a downward shift of its position. Specifically the ratio V_{max}/V_0 is approximately 1.8, 1.94 and 2.28 for $\emptyset_0$ equal to 0.1, 0.15 and 0.2 respectively. The form of these profiles is similar to that obtained by Stutz et al [15] who measured the velocity of a slurry (water with polypropylene spheres having a diameter of 3 mm and a density relative to water equal to 0.869) using a Pitot tube. Quantitative comparisons were not possible because this article does not specify the values of V_0 and $\emptyset_0$ for the reported experiments.

Results for turbulent flow

Figure 6 shows the axial evolution of the ice particles concentration distribution along the vertical diameter of the pipe for V_0 = 2 m/s and $\emptyset_0$ = 0.1 (as before this corresponds to a temperature of 267.56 K, i.e. slightly lower than the fusion temperature). The qualitative explanation of the corresponding results for laminar flow still apply and justify the increase of the ice concentration in the upper part of the pipe as well as its decrease in the lower part. It is important however to note that in the present case the concentration profile has not reached a form independent of the axial position as indicated by the difference between the profiles for z = 1.5 m and z = 2.95 m. This result shows that in the present case the development length for ice concentration is longer than the length of the pipe used in this study (L = 3 m).

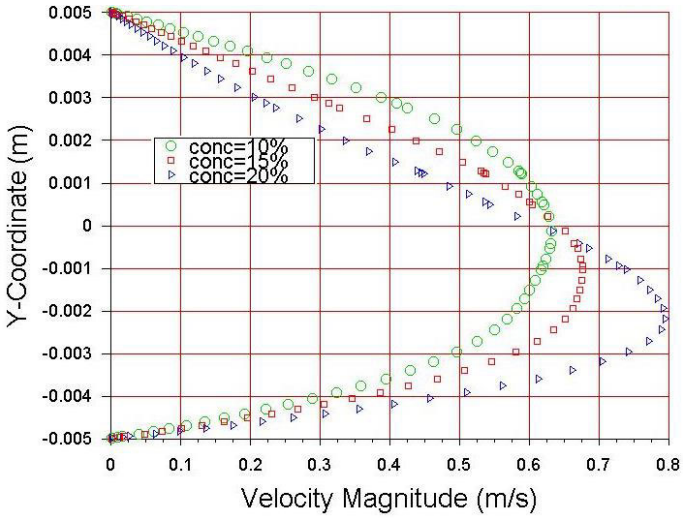

Fig. 5: Effect of $\emptyset_0$ on the fully developed velocity profile for V_0 = 0.35 m/s.

Figure 7 shows the corresponding iso-concentration lines at z = 2.95 m which as expected are symmetrical with respect to the vertical diameter of the pipe.

Figure 8 shows the corresponding axial evolution of the velocity profiles along the vertical diameter of the pipe. The overshoot is again present near the pipe inlet but beyond approximately z = 1.5 m the profile becomes independent of the axial position and attains a fairly flat form characteristic of turbulent flows. The hydrodynamically developed profile is very similar to the experimental and numerical results of Jihong Wang et al [4]. According to Figure 8 the ratio V_{max}/V_0 is approximately equal to 1.25 in the hydrodynamically developed region.

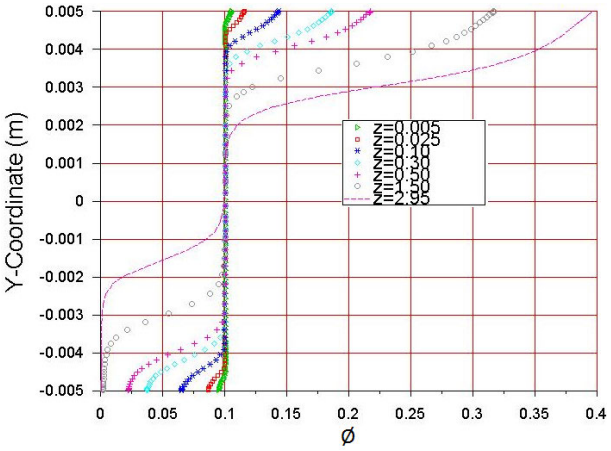

Fig. 6: Axial evolution of the concentration profile for V_0 = 2 m/s and $\emptyset_0$ = 0.1

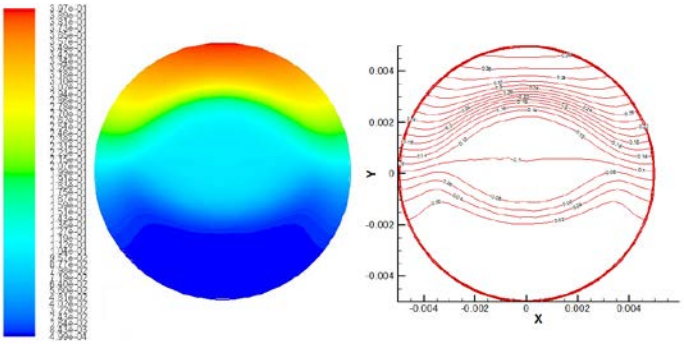

Fig. 7: Concentration distribution at z = 2.95 m for V_0 = 2 m/s and $\emptyset_0$ = 0.1

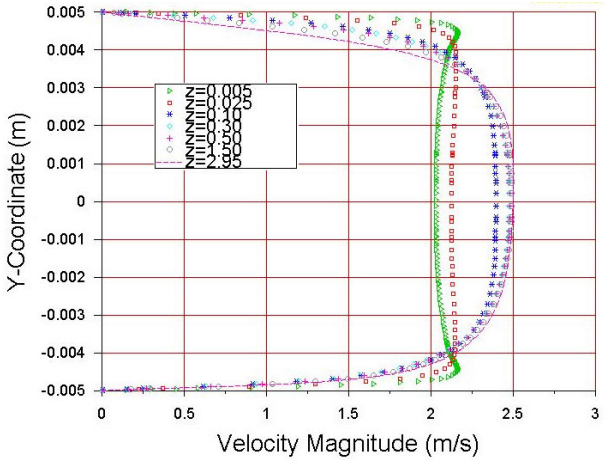

Fig. 8: Axial evolution of the velocity profile for V_0 = 2 m/s and $\emptyset_0$ = 0.1

Figure 9 shows the lines of constant velocity at z = 2.95 m which indicate that the velocity field is not symmetrical with respect to the horizontal diameter of the pipe. Specifically, for symmetrical positions with respect to this diameter the velocity in the upper part is slightly smaller. This is due to the increased concentration of ice particles in the upper part which causes an increase of the molecular viscosity. The corresponding decrease of the velocity is however small since the molecular viscosity is small compared to the turbulent viscosity.

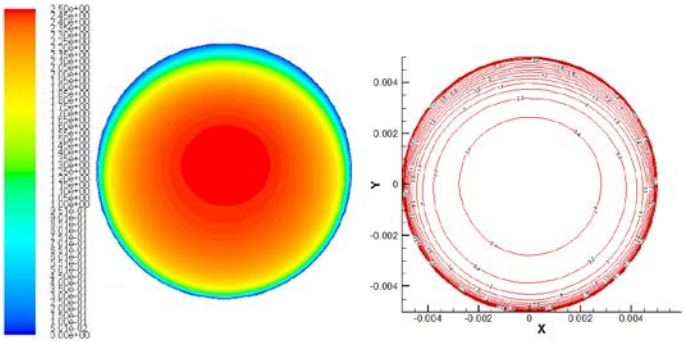

Fig. 9: Velocity distribution at z = 2.95 m for V_0 = 2 m/s and $\emptyset_0$ = 0.1

Figure 10 illustrates the effect of the inlet ice concentration on the concentration profile at z = 2.95 m for V_0 = 2 m/s. We note that the difference between the maximum concentration (which occurs at the top of the pipe) and the minimum concentration (which occurs at the bottom) is greatest for the smallest value of $\emptyset_0$ and smallest for the greatest value of $\emptyset_0$. Complete elimination of the ice from the bottom part of the pipe occurs only for the smallest value of $\emptyset_0$. Qualitatively these results are consistent with experimental observations [1].

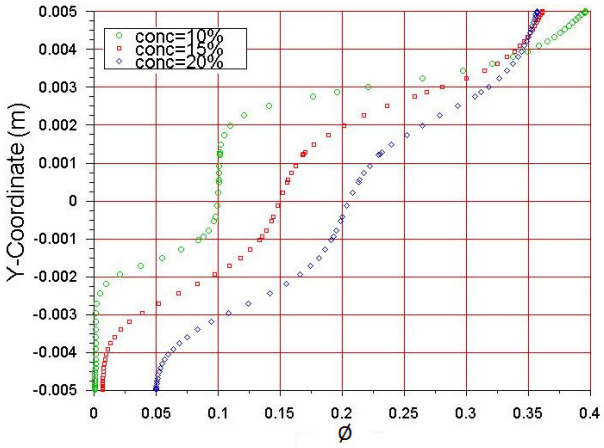

Fig. 10: Effect of $\emptyset_0$ on the concentration profile at z = 2.95 m for V_0 = 2 m/s.

Figure 11 illustrates the effect of the inlet ice concentration on the hydrodynamically developed velocity profile at z = 2.95 m for V_0 = 2 m/s. The maximum velocity increases slightly as the inlet concentration increases. It should be noted that the velocity at y = 0.004 m is smaller than at y = - 0.004 m. These results clearly illustrate that this profile is not symmetrical with respect to the pipe axis for the reasons explained in the discussion of Figure 9.

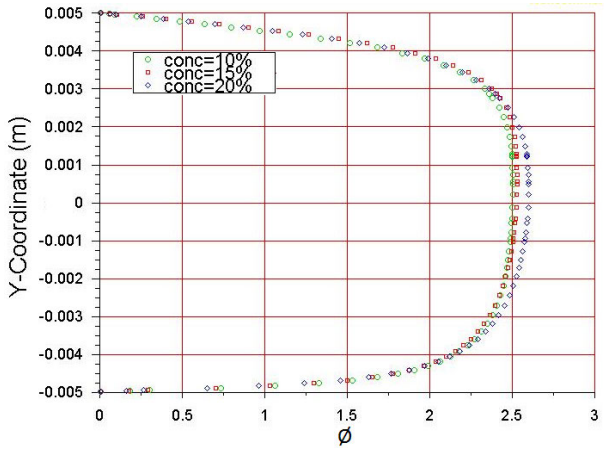

Fig. 11: Effect of $\emptyset_0$ on the velocity profile at z = 2.95 m for V_0 = 2 m/s.

Table 3 shows the average concentration of the ice particles for different cross sections normal to the pipe axis for turbulent flow with V_0 = 2 m/s and $\emptyset_0$ = 0.1. These values were calculated as explained earlier in the case of laminar flow. Even though they increase slightly in the direction of flow they are everywhere within less than 2% of the exact value (i.e. the concentration at the inlet). Therefore we consider that the model and its numerical solution are reliable.

Axial position z (m)	0.05	0.5	1.0	2.0	2.95
Average ice concentration (%)	10.01	10.05	10.08	10.12	10.16

Table 3: Validation of the constancy of the average ice concentration for turbulent flow

Comparison of laminar and turbulent results

For all simulations in this section the value of the inlet ice concentration is 10%. The results show velocity and concentration profiles along the vertical diameter of the pipe.

Figures 12 and 13 compare the normalized velocity profiles for laminar (V_0 = 0.2 m/s) and turbulent (V_0 = 2 m/s) flow at z = 0.5 m and z = 2.95 m respectively. The differences at both positions are striking. The maximum normalized velocity in the case of laminar flow is almost twice that of turbulent flow. The asymmetry with respect to the pipe's axis is much more pronounced in the case of laminar flow. Near the top and bottom the velocity increases much faster in the turbulent case. The relative importance of the wall shear stress for the top and bottom of each flow regime cannot be deduced from the corresponding velocity gradients because the viscosity is not the same at these positions. Further calculations are therefore required to evaluate the circumferential and axial distributions of the wall shear stress for each flow regime.

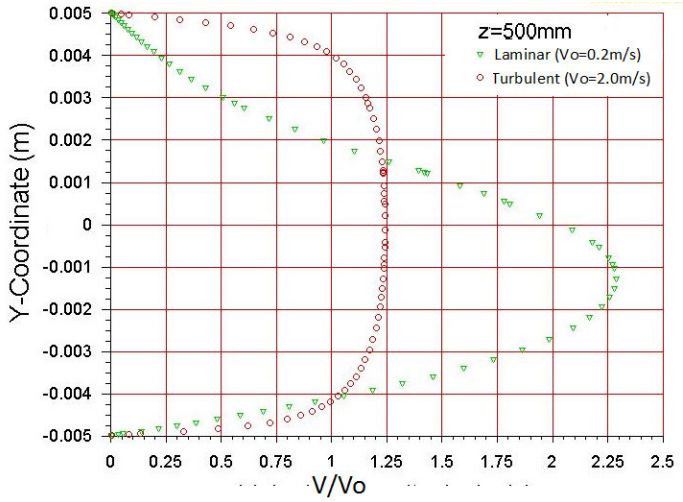

Fig. 12: Comparison of normalized velocity profiles for laminar and turbulent flow at z = 0.5 m

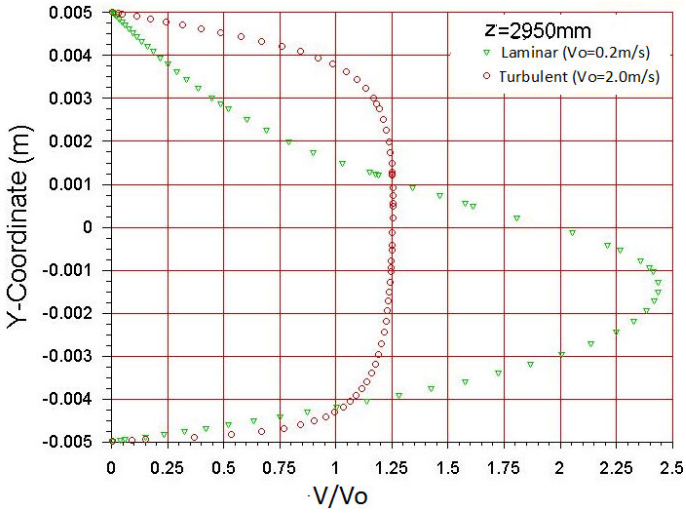

Fig. 13: Comparison of normalized velocity profiles for laminar and turbulent flow at z = 2.95 m

Figures 14 and 15 compare concentration profiles for laminar (V_0 = 0.2 m/s) and turbulent (V_0 = 2 m/s) flow at z = 0.5 m and z = 2.95 m respectively. Again the differences between laminar and turbulent results are striking. For laminar flow the lower part of the pipe does not contain any ice and elsewhere it increases almost linearly. For turbulent flow the concentration remains equal to the inlet value over an important part of the profile (more than half at z = 0.5 m and approximately 20% at z = 2.95 m). At z = 0.5 m the minimum ice concentration is still positive. At both positions the differences between the maximum and minimum concentrations are considerably higher in the case of laminar flow. These observations indicate that the ice concentration profile evolves much faster in the case of laminar flow. It therefore appears that turbulence slows down the effects of buoyancy and diffusion which act alone in the case of laminar flow and tends to maintain a relative uniformity of the ice concentration.

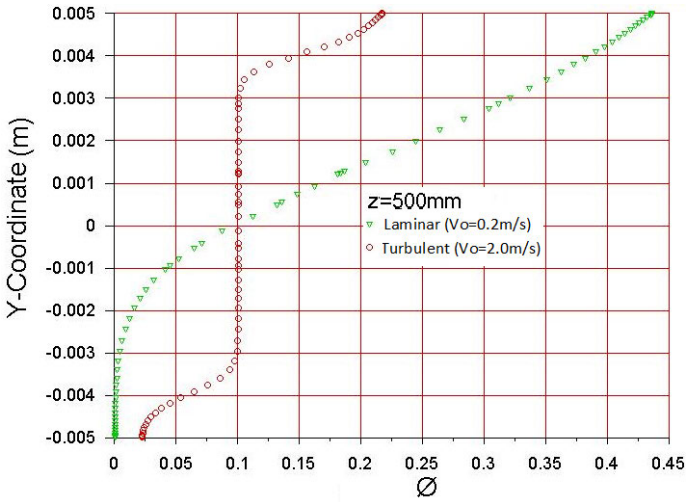

Fig. 14: Comparison of concentration profiles for laminar and turbulent flow at z = 0.5 m

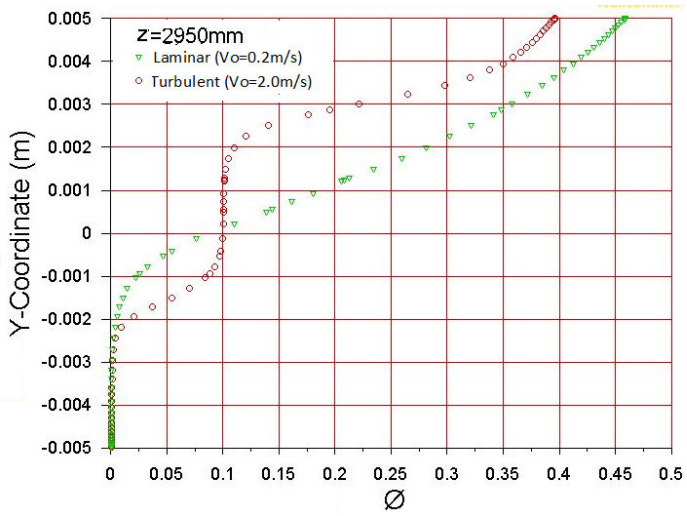

Fig. 15: Comparison of concentration profiles for laminar and turbulent flow at z = 2.95 m

CONCLUSIONS

The adopted single-phase model of isothermal ice slurry flow in a horizontal pipe is simpler than the two-phase models used in most other studies of this problem. Nevertheless its numerical predictions correctly reflect the experimentally determined effects for both laminar and turbulent conditions.

Specifically, for laminar flow the model shows that:

- The velocity distribution is not symmetrical with respect to the horizontal symmetry plane; the maximum velocity occurs below the pipe axis and increases significantly with the inlet ice concentration.
- As the slurry moves downstream the ice concentration increases in the upper part of the pipe; in the lower part ice particles eventually disappear completely; the difference between the maximum and minimum concentrations in a fixed cross-section increases with the inlet ice concentration.

For turbulent flow the model shows that:

- The shape of the velocity profile is essentially determined by the turbulence although it is not exactly symmetrical with respect to the horizontal symmetry plane; the effect of the inlet ice concentration on the hydrodynamically developed velocity distribution is very small.
- The ice concentration increases in the upper part of the pipe and it decreases in its lower part; the difference between the maximum and minimum concentrations in a fixed cross-section decreases when the inlet ice concentration increases.

The differences between the behavior of laminar and turbulent flows have been explained by considering the effect of ice concentration on the molecular dynamic viscosity of the slurry and its magnitude relative to the turbulent viscosity.

ACKNOWLEDGMENTS

This project is part of the R&D program of the NSERC Chair in Industrial Energy Efficiency established in 2006 at '*Université de Sherbrooke*'. The authors acknowledge the support of the Natural Sciences & Engineering Research Council of Canada, Hydro Québec, Rio Tinto Alcan and Canmet-Energy Research Center of Natural Resources Canada.

NOMENCLATURE

a	mean radius of ice particles
D	pipe diameter
d	mean diameter of ice particles
k	kinetic energy of turbulence
L	pipe length
N	particle flux
p	pressure
$\boldsymbol{Q}$	gravitational acceleration vector
Re	Reynolds number
T	temperature
$\boldsymbol{u}$	velocity vector
V	velocity component in z-direction
X	mass concentration
x,y,z	Cartesian coordinates
z^*	$= (z/D)/Re$
Greek letters	
$\dot{\gamma}$	shear rate
ε	dissipation rate
μ	dynamic viscosity
ρ	density
$\boldsymbol{\tau}$	stress tensor
Ø	volumetric concentration
Subscripts	
0	inlet
i	ice
is	ice slurry
l	water-additive mixture

REFERENCES

[1] Kauffeld M., Kawaji M. & Egolf P., 2005, "Handbook on Ice Slurries – Fundamentals and Engineering", International Institute of Refrigeration (IIF/IIR), France.

[2] Kitanovski A. & Poredos A., 2002, "Concentration distribution and viscosity of ice-slurry in heterogeneous flow", Internationl Journal of Refrigeration, 25(6), pp. 827-835.

[3] Kitanovski A., Vuarnoz D., Ata-Caesar D., Egolf P. W., Hansen T. & Doetsch C., 2005, "The fluid dynamics of ice slurry, International Journal of Refrigeration, 28(1), pp. 37–50.

[4] Jihong Wang, Shugang Wang, Tengfei Zhang & Yuntao Liang, 2013, "Numerical Investigation of Ice Slurry Isothermal Flow In Various Pipes", International Journal of Refrigeration, 36(1), pp. 70-80.

[5] Niezgoda-Zelasko B. & Zalewski W., 2006, "Momentum transfer of ice slurry flows in tubes, modeling", International Journal of Refrigeration, 29(3), pp. 429-436.

[6] Phillips R. J., Armstrong R. C., Brown R. A., Graham A. L. & Abbot J. R., 1992, "A Constitutive Equation for Concentrated Suspensions that Accounts for Shear-Induced Particle Migration", Physics of Fluids A, 4(1), pp. 30-40.

[7] Leighton D. & Acrivos A., 1987, "The Shear Induced Migration of Particles in Concentrated Suspensions", Journal of Fluid Mechanics, 181, pp. 415-439.

[8] Richardson J. F. & Zaki W. N., 1954, “Sedimentation and Fluidization: Part 1”, Trans. Inst. Chem. Engrs., 32, pp. 35-53.
[9] Revay J. M. & Higdon J. J. L., 1992, “Numerical Simulation of Polydisperse Sedimentation: Equal-Size Spheres”, Journal of Fluid Mechanics, 243, pp. 15-32.
[10] Bui A. & Rudman M., 2003, “Modeling of viscous resospension using a one-field description of multiphase flows”, The International Conference on CFD in Minerals and Process Industries (CSIRO), Melbourne, Australia, pp. 10-42.
[11] Renaud-Boivin S., Poirier M. & Galanis N., 2012, “Experimental Study of Hydraulic and Thermal Behavior of an Ice Slurry in a Shell and Tube Heat Exchanger”, Experimental Thermal and Fluid Science, 37, pp. 130-141.
[12] ASHRAE, 2005, “Handbook of Fundamentals”, Atlanta GA.
[13] Nascimento S.C.C., Macedo E.N. & Quaresmo J.N.N., 2006, “Generalized Integral Transform Solution for Hydrodynamically Developing Non-Newtonian Flows in Circular Tubes”, J. of the Braz. Soc. of Mech. & Eng., 28(1), pp. 125-130.
[14] Liu J., 1974, “Flow of Bingham Fluid in the Entrance Region of an Annular Tube”, M. S. Thesis, University of Wisconsin-Milwaukee, USA.
[15] Stutz B., Reghem P. & Martinez O., “Flow of Slurries of Particles with Density Close to that of Water” Consulted online April 3, 2013 at: http://docsmartinez.free.fr/NO_vi.PDF